This is a repository copy of *Radial and rotational velocities of young brown dwarfs and very low-mass stars in the Upper Scorpius OB association and the ρ Ophiuchi cloud core*.

White Rose Research Online URL for this paper:
http://eprints.whiterose.ac.uk/144704/

Version: Published Version

Article:
Kurosawa, R., Harries, T.J. and Littlefair, S.P. orcid.org/0000-0001-7221-855X (2006) Radial and rotational velocities of young brown dwarfs and very low-mass stars in the Upper Scorpius OB association and the ρ Ophiuchi cloud core. Monthly Notices of the Royal Astronomical Society, 372 (4). pp. 1879-1887. ISSN 0035-8711

https://doi.org/10.1111/j.1365-2966.2006.11005.x

This article has been accepted for publication in Monthly Notices of the Royal Astronomical Society © 2006 The Authors. Journal compilation © 2006 RAS. Published by Oxford University Press on behalf of the Royal Astronomical Society. All rights reserved

Reuse
Items deposited in White Rose Research Online are protected by copyright, with all rights reserved unless indicated otherwise. They may be downloaded and/or printed for private study, or other acts as permitted by national copyright laws. The publisher or other rights holders may allow further reproduction and re-use of the full text version. This is indicated by the licence information on the White Rose Research Online record for the item.

Takedown
If you consider content in White Rose Research Online to be in breach of UK law, please notify us by emailing eprints@whiterose.ac.uk including the URL of the record and the reason for the withdrawal request.

eprints@whiterose.ac.uk
https://eprints.whiterose.ac.uk/

Mon. Not. R. Astron. Soc. **372,** 1879–1887 (2006) doi:10.1111/j.1365-2966.2006.11005.x

Radial and rotational velocities of young brown dwarfs and very low-mass stars in the Upper Scorpius OB association and the ρ Ophiuchi cloud core

Ryuichi Kurosawa,[1★] Tim J. Harries[1] and S. P. Littlefair[2]

[1]*School of Physics, University of Exeter, Stocker Road, Exeter EX4 4QL*
[2]*Department of Physics and Astronomy, University of Sheffield, Sheffield S3 7RH*

Accepted 2006 August 26. Received 2006 August 24; in original form 2006 June 20

ABSTRACT

We present the results of a radial velocity (RV) survey of 14 brown dwarfs (BDs) and very low-mass (VLM) stars in the Upper Scorpius OB association (UScoOB) and three BD candidates in the ρ Ophiuchi dark cloud core. We obtained high-resolution echelle spectra at the Very Large Telescope using the Ultraviolet and Visual Echelle Spectrograph (UVES) at two different epochs for each object, and measured the shifts in their RVs to identify candidates for binary/multiple systems in the sample. The average time separation of the RV measurements is 21.6 d, and our survey is sensitive to the binaries with separation <0.1 au. We found that four out of 17 objects (or 24^{+16}_{-13} per cent by fraction) show a significant RV change in 4–33 d time-scale, and are considered as binary/multiple 'candidates'. We found no double-lined spectroscopic binaries in our sample, based on the shape of cross-correlation curves. The RV dispersion of the objects in UScoOB is found to be very similar to that of the BD and VLM stars in Chamaeleon I (Cha I). We also found the distribution of the mean rotational velocities ($v \sin i$) of the UScoOB objects is similar to that of the Cha I, but the dispersion of $v \sin i$ is much larger than that of the Cha I objects.

Key words: binaries: spectroscopic – stars: formation – stars: low-mass, brown dwarfs – planetary systems: formation.

1 INTRODUCTION

Most stars are member of binary systems and it is therefore important that a complete star formation theory be able to predict the binary fraction, period distribution and mass-ratio distribution of stellar objects across a wide range of masses. Furthermore, the study of individual binary systems is the only direct means to determine fundamental stellar properties such as stellar masses and radii.

Recent high-resolution imaging studies of brown dwarfs (BDs) and very low-mass (VLM) stars have placed strong constraints on binaries with separations of ∼1–100 au. For example, *Hubble Space Telescope* (*HST*) observations of α Per and the Pleiades indicates a binary fraction (f) of >10 per cent with a bias towards separations (a) of less than 15 au, and a mass ratio (q) of >0.7 (Martín et al. 2003) for objects around and below the hydrogen burning limit (see also Bouy et al. 2006). A similar lack of wide binaries was found in the field T-dwarf study (Burgasser, McElwain & Kirkpatrick 2003), while $f \approx$ 15 per cent (for the field objects with 0.03–0.1 $M_\odot$ and M8.0–L0.5) was determined by Close et al. (2003) using the adaptive optics at Gemini North. They also found the vast majority of systems have a semimajor axis <20 au (see also Siegler et al. 2005 but note too the results of Luhman 2004). An *HST* study of more than 80 field late M and L dwarfs (Gizis et al. 2003) indicated $f \approx 15$ per cent with separations in the range of 1.6–16 au. For a small (12) sample of BDs and VLM stars (0.04–0.1 $M_\odot$) in Upper Scorpius OB association (UScoOB), Kraus, White & Hillenbrand (2005) found $f = 25^{+16}_{-8}$ per cent for 5 au $< a <$ 18 au by using a similar imaging technique. More recently, Basri & Reiners (2006), combined with the results of earlier works, found the upper limit of the overall binary fraction for VLM stars of 26 ± 10 per cent.

Using a Monte Carlo simulation, the data from radial velocity (RV) surveys available in the literature, and by carefully considering the sensitivity and sampling biases, Maxted & Jeffries (2005) found an overall BD/VLM binary frequency of 32–45 per cent assuming $f = 15$ per cent for $a > 2.6$ au. A recent photometric study (Pinfield et al. 2003) of low-mass objects in Pleiades and Praesepe suggested, albeit indirectly, f as large as 50 per cent which would only be compatible with direct imaging studies if 70–80 per cent of those binaries have $a < 1$ au. For a more comprehensive review of the current status of BD/VLM binary fraction and the separation distribution, readers are refer to a recent review of multiplicity studies by Burgasser et al. (2006).

The extensive imaging surveys provide excellent observational constraints on wider BD + BD binaries, but it is now necessary to search for shorter period BD + BD binaries systematically.

★E-mail: rk@astro.ex.ac.uk

© 2006 The Authors. Journal compilation © 2006 RAS

Downloaded from https://academic.oup.com/mnras/article-abstract/372/4/1879/1192749 by University of Sheffield user on 08 April 2019

Binaries with the separation of less than 1 au are not resolved by current imaging techniques, but will be detectable as spectroscopic binaries, providing the mass ratio is not too extreme, and velocity separation is large enough. The first BD + BD spectroscopic binary, PPl 15 (Basri & Martín 1999), showed a double-peaked cross-correlation function with a maximum velocity separation of >70 km s^{-1}. The binary was found to have an eccentric orbit ($e = 0.4$) with a period of ~5.8 d. Basri & Martín (1999) suggested that the formation process of substellar objects is biased towards smaller separation binaries based on the short period of PPl 15 and the lack of Pleiades BD binaries with separations >40 au. Note that the median separation of binaries with solar-type primaries is 30 au (Duquennoy & Mayor 1991). Pioneering work on the RVs of BDs and VLMs are presented by Guenther & Wuchterl (2003), Kenyon et al. (2005) and Joergens (2006b) who found a several binary candidates; however, the orbital parameters and masses of binaries remains unknown because the follow-up spectroscopic monitoring is lacking or is still being undertaken. In addition to the follow-up observations, the number of BDs and VLM star binary candidates needs to be increased in order to have better statistics on short-period binary parameters.

The first BD + BD eclipsing binary (2MASS J0532184−J0546085) was discovered by Stassun, Mathieu & Valenti (2006) from the *I*-band photometric monitoring of the system. Combining their light curves and the results from the follow-up RV measurements, they were able to determine the precise orbital and physical parameters of the system. The projected semimajor axis and the period of the binary are found as 0.0398 ± 0.0010 au and 9.779 621 ± 0.000 042 d, respectively.

The separation distribution of BD/VLM binaries is critical to understanding their origin. There are two main models for the formation of BDs and VLM stars: first, they have low masses because they form in low-mass, dense molecular cloud cores (e.g. Padoan & Nordlund 2002); secondly, BD/VLM objects have low masses because they are ejected from the dense core in which they form via dynamical interactions in multiple system, cutting off their accretion before they have reached stellar masses (Reipurth & Clarke 2001; Bate, Bonnell & Bromm 2002a). Alternatively, there is a third model in which a free-floating BD or planetary-mass object can be formed in the process of the photo-evaporation (e.g. McCaughrean & Andersen 2002; Whitworth & Zinnecker 2004) with the outer layers of a pre-stellar core (~0.2 $M_{\odot}$) removed by the strong radiation pressure from the nearby massive OB stars before the accretion on to the protostar at core centre occurs.

Due to the dynamical interaction involved in the second model, BD/VLM binaries that survive are generally expected to have small separations. In the first model, wider binaries may be expected to be more common. Bate, Bonnell & Bromm (2002b) suggested that close binaries (a < 10 au) do not form directly, but result from hardening of wider systems though a combination of dynamical interactions, accretion and interactions with circumbinary discs. If BD/VLM binaries have formed through such mechanisms, one would not expect to find binaries with 1–10 au separations without also finding many with separation <1 au. If an absence/rarity of binaries with 1 au were found, it may support the idea that they are ejected quickly from multiple systems before they have undergone the interactions that shorten their periods.

Our immediate aim is to identify spectroscopic and close BD/VLM binaries using the high-resolution echelle spectroscopy at two epochs. This experiment is sensitive to VLM binaries with separations of <0.1 au which corresponds to a period of ~10 d. A larger sample of candidates will enable us to measure the binary fraction of these short-period/close binaries (once confirmed), and address whether there is a significant population of 'hidden' VLM companions. The long-term goal of this project to follow up the binary candidates found in this paper by spectroscopically monitoring them over different time-scales, enabling us to obtain the RV curves and their minimum masses.

In Section 2, we describe the observations and the data reduction. The results of RV and rotational velocity ($v \sin i$) measurements are presented in Section 3. We discuss the binary/multiplicity fraction indicated by our RV survey in Section 4, and give our conclusions in Section 5.

2 OBSERVATIONS

Our sample consists of 18 young, VLM objects: 15 objects in the UScoOB ($d \approx 145$ pc; de Zeeuw et al. 1999) from the list of Ardila, Martín & Basri (2000) and three objects in the ρ Ophiuchi cloud core ($d \approx 150$ pc; de Zeeuw et al. 1997) from Luhman & Rieke (1999). The spectral type of the objects range between M5 and M8.5, and the age < ~10 Myr (Luhman & Rieke 1999; Ardila et al. 2000; Muzerolle et al. 2003; Kraus et al. 2005). The sample is not complete, and the selection was solely based on brightness and the observability. The basic properties of the targets based on the literature is summarized in Table 1.

We obtained high-resolution spectra with the Kueyen telescope of the Very Large Telescope (VLT–Cerro Parnal, Chile) using the Ultraviolet and Visual Echelle Spectrograph (UVES). The observations were carried out between 2004 April 5 and May 17 in service mode. For each object, spectra were obtained at two different epochs separated by 4–33 d. For each object on a given night, two separate spectra were obtained consecutively. This allows us to derive more reliable uncertainty estimates in the RV values of our targets (cf. Joergens 2006b). The data were obtained using the red arm of UVES with two mosaic CCDs (EEV + MIT/LL with 2000 × 4000 pixels). The wavelength coverage of 6708–10 250 Å and the spectral resolution $R \approx 40\,000$ were used. The slit width and length of 1 and 12 arcsec were used, respectively, with a typical seeing of 0.8 arcsec.

The data were reduced via the standard ESO pipeline procedures for UVES echelle spectra. In summary, the data were corrected for bias, interorder background, sky background, sky emission lines and cosmic ray hits. They were then flattened, optimally extracted, and finally the different orders were merged. No binning was performed to achieve high resolution required for the RV measurements. The wavelength was calibrated using the thorium–argon arc spectra with a typical value of the s.d. of the dispersion solution of 5 mÅ which corresponds to 0.2 km s^{-1} at the central wavelength 8600 Å. However, the autoguiding of the telescope keeps the star at the centre of the slit with about a tenth of the FWHM (1 km s^{-1}) which sets the upper limit for the systematic error in the RV measurements (Bailer-Jones 2004) . In fact, we find that any systematic error is negligible compared to the random error associated with our RV measurements (see Section 3.1). A typical signal-to-noise ratio (S/N) per wavelength bin of the spectra is about 15, and the heliocentric velocity correction was applied to the final spectra.

In addition to the main targets in Table 1, we also obtained the spectra of LHS 49 (on 2004 April 17) and HD 140538 (on 2004 May 06), which are the RV template and the RV standard stars, respectively. These data were obtained using the same telescope and the same instrumental set-up as for our main targets. The S/N of the both objects were about 60.

Downloaded from https://academic.oup.com/mnras/article-abstract/372/4/1879/1192749 by University of Sheffield user on 08 April 2019

Table 1. Summary of known properties of the targets from literature.

Object	Spectral type	Mass ($M_\odot$)	RV (km s^{-1})	$v \sin i$ (km s^{-1})	Known multiple?
GY 5	M7[c]	0.07[d]	-6.3 ± 1.9[d]	16.8 ± 2.7[d]	No
GY 141	M8.5[a]	0.02[d]	–	6.0[f]	No
GY 310	M8.5[c]	0.08[a,d]	–	10.0[f]	No
USco 40	M5[b]	0.1[b]	–	37.5[f]	No
USco 53	M5[b]	0.1[b]	–	45.0[f]	No
USco 55	M5.5[b]	$0.10 + 0.07$[e]	–	12.0[f]	Visual [e]
USco 66	M6[b]	$0.07 + 0.07$[e]	-4.4 ± 0.6[d]	27.5[f]	Visual [e]
USco 67	M5.5[b]	0.10[e]	–	18.0[f]	No
USco 75	M6[b]	0.07[e]	-5.6 ± 1.1[d]	63.0[f]	No
USco 100	M7[b]	0.05[e]	-8.9 ± 0.6[d]	50.0[f]	No
USco 101	M5[b]	0.05[b]	–	–	No
USco 104	M5[b]	0.05[b]	–	16.0[f]	No
USco 109	M6[b]	$0.07 + 0.04$[e]	-3.8 ± 0.7[d]	6.0[f]	Visual [e]
USco 112	M5.5[b]	0.1[e]	–	8.0[f]	No
USco 121	M6[b]	0.02[b]	-38.9 ± 1.0[d]	–	No
USco 128	M7[b]	0.05[e]	-3.0 ± 1.6[d]	0.0[f]	No
USco 130	M7.5[e]	0.04[e]	–	14.0[f]	No
USco 132	M7[b]	0.05[e]	-8.2 ± 1.1[d]	–	No

[a]Luhman & Rieke (1999) (original list for ρ Oph); [b]Ardila et al. (2000) (original list for UScoOB); [c]Wilking, Greene & Meyer (1999); [d]Muzerolle et al. (2003); [e]Kraus et al. (2005) and [f]Mohanty et al. (2005).

3 RESULTS

3.1 Radial velocities

The RVs of each object were determined by using the cross-correlation function of the object spectrum with that of a template star which has a similar spectral type. By visual inspection, the wavelength ranges used for the cross-correlation calculations are chosen by avoiding the regions of spectra affected by the telluric lines, and defects and fringes (in near-infrared) of the CCDs. The RVs of objects with respect to the template are obtained by measuring the location of the peak in the cross-correlation function. The location of the peak is determined by fitting the section of the cross-correlation function around the peak by a second-order polynomial. LHS 49 (Proxima Cen, M5.5) was chosen as the template for this purpose. The heliocentric RV of the template object LHS 49 was obtained by measuring the wavelength shifts of the prominent photospheric absorption features K I $\lambda\lambda$7664.911, 7698.974. This gives us $RV_{LHS\,49} = -22.6 \pm 0.5$ km s^{-1}, which is in good agreement with the earlier measurement of García-Sánchez et al. (2001) who found $RV_{LHS\,49} = -21.7 \pm 1.8$ km s^{-1}. The heliocentric RV of each object can be then calculated by adding $RV_{LHS\,49}$ with the RV of each object with respect to LHS 49. In the following measurements of the heliocentric RVs, our measurement ($RV_{LHS\,49} = -22.6 \pm 0.5$ km s^{-1}) will be used for consistency.

Before applying the cross-correlation technique to our main targets, we have applied the technique to the RV standard HD 140538 (G2.5V) for which an high-accuracy RV measurement via the fixed-configuration, cross-dispersed echelle spectrograph Elodie (Baranne et al. 1996) is available. This was done so to ensure not only the validity of the cross-correlation technique, but also the validity of the wavelength calibration. In this test, we found the heliocentric $RV_{HD\,140538} = 19.17 \pm 0.40$ km s^{-1} which is in good agreement with the Elodie RV measurement of 19.00 ± 0.05 km s^{-1} (Udry, Mayor & Queloz 1999). Note that the uncertainty in $RV_{HD\,140538}$ was computed by combining (in quadrature) the uncertainty (0.4 km s^{-1}) in the heliocentric RV of the template star HD 74497 (G3V) and the uncertainty in the relative RV of HD 140538 (0.02 km s^{-1}), measured by cross-correlation with the template star. Clearly, the former dominates in the uncertainty of $RV_{HD\,140538}$ shown above. The uncertainty in the heliocentric RV of the template is rather large because it was determined from a few photospheric lines.

The results of the heliocentric RV measurements (from two epochs for each object) are summarized in Table 2 along with their uncertainties. The uncertainties listed in columns 4 and 6 include the uncertainty of the absolute RV of the template star, added in quadrature with the uncertainty found from the cross-correlation analysis. On the other hand, the uncertainties in the relative RVs (σ_{RRV}) listed in column 5 of the table *do not* include the uncertainty of the template star. It is σ_{RRV} that is relevant for the identification of RV variable objects.

To determine the σ_{RRV}, we have used the following procedure: (1) add random Gaussian deviate noise to the object spectra using the corresponding variance spectra,[1] (2) compute the cross-correlation curve using the spectra with added noise and the template, (3) measure the RV by locating the peak, (4) repeat steps 1–3 for 100 times and compute the s.d. of the 100 RV values. This should provide a good estimate of uncertainties in RVs cased by the uncertainties in the flux levels. We also estimated the RV uncertainties using the s.d. values on the mean of the two independent RV measurements obtained from the two consecutive spectra taken on the same night (cf. Joergens 2006b). We found that these estimates agreed well with those obtained from the Monte Carlo method. The 'average' RVs ($\overline{RV}$) of the two epochs are also given in Table 2.

For each object and for each RV measurement, the deviations (ΔRV) from the average RV are computed and summarized in Fig. 1 along with their uncertainties (σ_{RRV}) in order to aid the identification of multiplicity candidates. Note that in computing ΔRV we do not require the knowledge of absolute/heliocentric

[1] Defined by the variance of the χ^2 fit to the signal obtained during optimum extraction (cf. Horne 1986).

© 2006 The Authors. Journal compilation © 2006 RAS, MNRAS **372,** 1879–1887

Downloaded from https://academic.oup.com/mnras/article-abstract/372/4/1879/1192749 by University of Sheffield user on 08 April 2019

Table 2. Summary of the observations, the heliocentric RVs from two-epoch and the average rotational velocities ($v \sin i$). The uncertainties of relative RVs ($\sigma_{\rm RRV}$) with respect to the template star LHS 049 and the average RVs ($\overline{\rm RV}$) are also given. NB: The uncertainties listed along with the heliocentric RVs in column 4 and 6 include the uncertainty in the heliocentric RV of the template star, but $\sigma_{\rm RRV}$ in column 5 do not.

Object	Date	HJD 245 3100	RV (km s^{-1})	$\sigma_{\rm RRV}$ (km s^{-1})	$\overline{\rm RV}$ (km s^{-1})	$v \sin i$ (km s^{-1})
GY 5	2004 April 24	20.719 8440	−6.77 ± 2.02	1.96		
	2004 May 07	33.772 1938	−6.02 ± 0.85	0.68	−6.39 ± 2.19	16.5 ± 0.6
GY 141	2004 May 10	36.671 2108	−4.15 ± 0.63	0.38		
	2004 May 17	43.668 3007	−3.46 ± 0.66	0.43	−3.81 ± 0.91	4.4 ± 1.4
GY 310	2004 April 24	20.837 3504	−5.27 ± 0.92	0.77		
	2004 May 09	35.822 4052	−8.19 ± 0.71	0.51	−6.73 ± 1.16	11.1 ± 6.0
USco 40	2004 April 05	1.766 1754	−7.34 ± 0.52	0.15		
	2004 May 07	33.762 0554	−6.28 ± 0.52	0.15	−6.81 ± 0.74	34.2 ± 0.5
USco 53	2004 April 04	0.903 6653	−8.27 ± 0.70	0.50		
	2004 May 02	28.739 4676	−7.22 ± 0.63	0.39	−7.75 ± 0.95	40.0 ± 0.6
USco 55	2004 April 05	1.842 2807	−6.21 ± 0.50	0.04		
	2004 May 02	28.814 1198	−6.55 ± 0.50	0.06	−6.38 ± 0.71	22.9 ± 0.8
USco 66	2004 April 05	1.797 2634	−7.24 ± 0.95	0.81		
	2004 May 02	28.795 6003	−8.38 ± 1.32	1.22	−7.81 ± 1.63	25.9 ± 1.2
USco 67	2004 April 05	1.718 8620	−7.07 ± 0.67	0.44		
	2004 May 02	28.711 3799	−5.70 ± 0.58	0.30	−6.38 ± 0.88	18.4 ± 0.4
USco 75	2004 April 04	0.884 0376	−6.80 ± 0.70	0.50		
	2004 May 07	33.606 5432	−6.16 ± 0.78	0.60	−6.48 ± 1.05	55.6 ± 3.0
USco 100	2004 April 06	1.817 9138	−7.37 ± 0.67	0.44		
	2004 May 02	28.775 2928	−7.47 ± 0.62	0.36	−7.42 ± 0.91	43.7 ± 3.2
USco 101	2004 April 04	0.812 0734	−3.25 ± 0.66	0.44		
	2004 May 02	28.659 1660	−5.03 ± 0.60	0.32	−4.14 ± 0.89	19.1 ± 0.3
USco 104	2004 April 04	0.785 0385	−7.05 ± 0.61	0.35		
	2004 May 02	28.634 9480	−7.62 ± 0.57	0.27	−7.33 ± 0.83	16.7 ± 0.4
USco 109	2004 April 05	1.745 3989	−4.72 ± 0.50	0.07		
	2004 May 07	33.630 4878	−4.70 ± 0.51	0.09	−4.71 ± 0.72	8.6 ± 1.2
USco 112	2004 April 04	0.855 2168	−2.95 ± 0.50	0.05		
	2004 May 07	33.582 6368	−3.41 ± 0.51	0.07	−3.18 ± 0.71	5.8 ± 1.2
USco 121	2004 April 24	20.705 9408	−40.76 ± 0.90	0.74		
	2004 May 02	28.696 9641	−42.48 ± 0.54	0.20	−41.62 ± 1.04	17.6 ± 1.3
USco 128	2004 May 13	39.797 8276	−7.03 ± 0.51	0.09		
	2004 May 17	43.610 8024	−6.32 ± 0.51	0.10	−6.68 ± 0.72	3.6 ± 1.1
USco 130	2004 May 09	35.772 4090	−3.92 ± 0.94	0.80		
	2004 May 13	39.853 8830	−3.90 ± 0.67	0.45	−3.91 ± 1.16	15.2 ± 1.1
USco 132	2004 May 13	39.826 8683	−6.68 ± 0.53	0.18		
	2004 May 17	43.639 1138	−6.61 ± 0.54	0.20	−6.64 ± 0.76	9.1 ± 0.7

RVs, but only the relative velocities (with respect to a template). We also cross-correlated object spectra from the two epochs (instead of using the spectra of the template LHS 49) in order to find ΔRV. The resulting cross-correlation functions were found to be too noisy (due to the relatively low S/N in the object spectra) for the peak positions of the cross-correlation curves to be reliably located.

To identify an object with a RV variation with a statistical significance from our sample, we apply the method described by Maxted & Jeffries (2005), which we briefly summarize next, to our data. There are three steps in this method: (1) compute the χ^2 by fitting the two-epoch RV data for each object with a constant function (a zeroth-order polynomial), (2) compute the corresponding χ^2 probability (p), (3) designate the object as a non-constant RV object or a binary candidate if $p < 10^{-3}$ (0.1 per cent). When computing χ^2, we use the uncertainties in the relative RV ($\sigma_{\rm RRV}$). The number of degree of freedom in the fitting procedure is obviously 1. A similar method was also used in a recent RV survey of VLM stars by Basri & Reiners (2006).

We have computed p for all the objects (Table 3), and have plotted the results as a histogram of $-\log p$, shown in Fig. 2 (excluding the non-member USco 121; see explanation later). The figure clearly shows two distinctive populations: one on the left-hand side (with small $-\log p$ values) occupied by the RV constant objects, and the other on the right-hand side (with the large $-\log p$ values) occupied by the RV variable candidates. The expected distribution of p computed consistently with our uncertainty measurements is also shown in the same figure. The RV constant population on the left-hand side reasonably matches the expected curve. To quantify this point, we compute the χ^2 probability to test the goodness of the fit of the expected distribution to the histogram. We restrict the fit to the first four bins from the left-hand side ($0 < -\log_{10} p < 2$) of the histogram since the objects in the second bin from the right-hand side ($2.5 < -\log_{10} p < 3$) are 'potentially' RV variable, although we have flagged them as the RV-constant objects. In this analysis, we find the probability of 0.5 which indicates that the fit is reasonable. Further, if we renormalized the expected distribution, accounting for that fact we neglected the objects in the second bin from the

Downloaded from https://academic.oup.com/mnras/article-abstract/372/4/1879/1192749 by University of Sheffield user on 08 April 2019

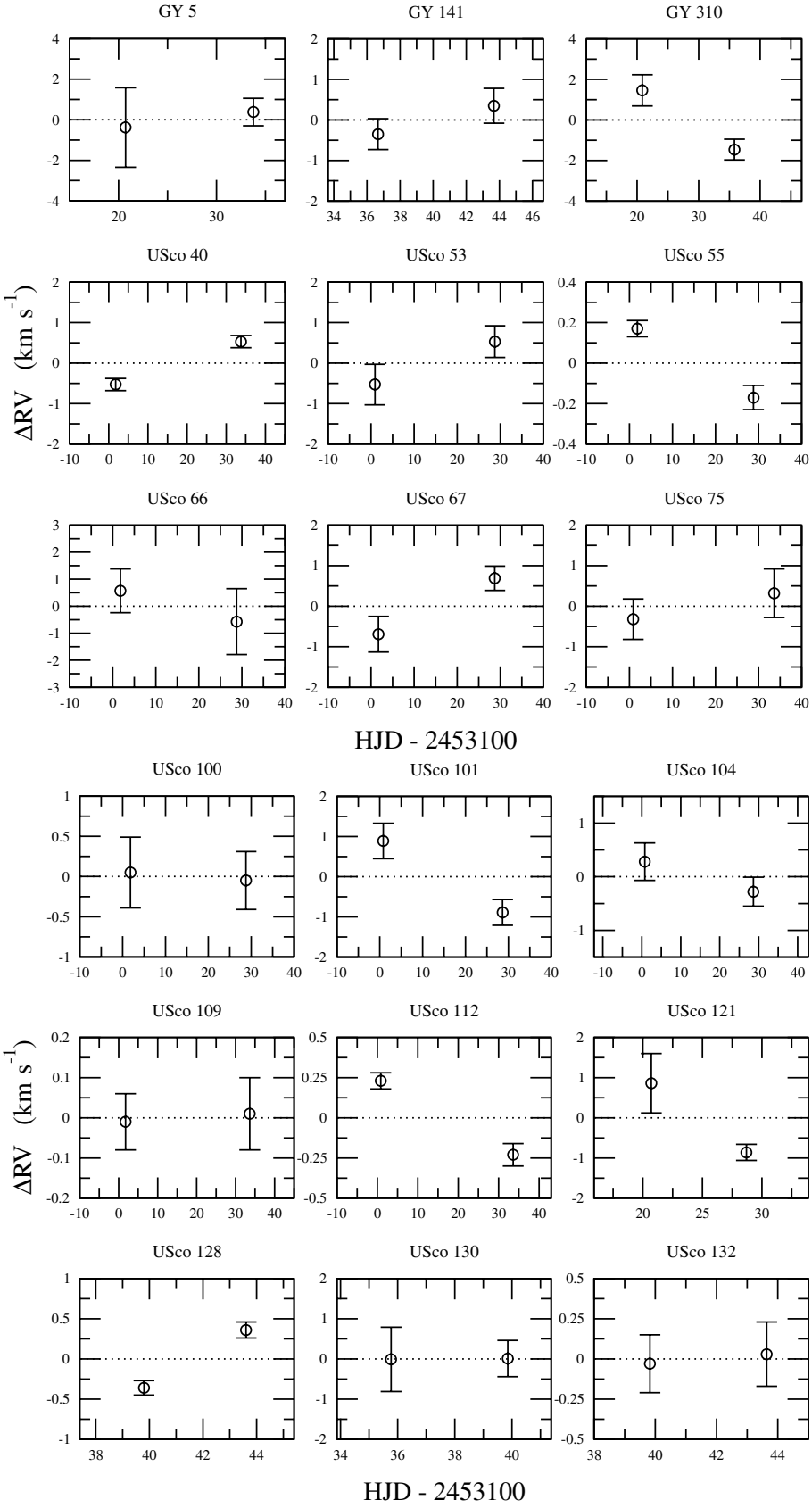

Figure 1. Relative RVs of objects measured in two different epochs. The vertical axes indicate the amount of deviation (ΔRV) from the 'average' RV ($\overline{\mathrm{RV}}$) in Table 2, and the horizontal axes indicate the time of the observation in heliocentric Julian Date (HJD). The objects are considered to have a non-constant RV when the error bars of two data points do not overlap each other. The non-constant RV objects are considered as binary/multiple candidates.

Downloaded from https://academic.oup.com/mnras/article-abstract/372/4/1879/1192749 by University of Sheffield user on 08 April 2019

Table 3. The χ^2 probabilities (p) of each object being a RV constant, listed in ascending order of p. The ellipses represent the boundary ($p = 10^{-3}$) between RV constant objects and RV variable objects.

Object ID	p
USco 112	8.9×10^{-8}
USco 128	1.3×10^{-7}
USco 40	5.8×10^{-7}
USco 55	2.4×10^{-6}
...	...
USco 101	1.1×10^{-3}
GY 310	1.6×10^{-3}
USco 67	1.0×10^{-2}
USco 53	9.8×10^{-2}
USco 104	2.0×10^{-1}
GY 141	2.3×10^{-1}
USco 75	4.1×10^{-1}
USco 66	4.4×10^{-1}
GY 5	7.2×10^{-1}
USco 132	7.9×10^{-1}
USco 100	8.6×10^{-1}
USco 109	8.6×10^{-1}
USco 130	9.8×10^{-1}

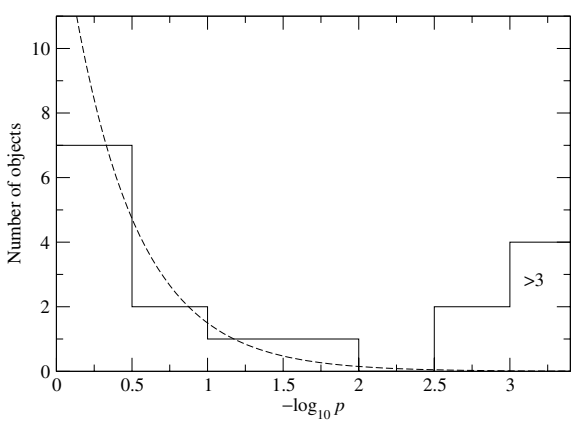

Figure 2. Histogram of the χ^2 probability (p) for fitting the observed (relative) RV values with a constant (a horizontal line). The constant used in the fit is determined from the weighted mean of the two RV measurements for each object. The objects with $p < 10^{-3}$ are identified as *non-constant* or *multiple*, which appear in the rightmost bin in the histogram. There are four objects which satisfy this condition. The expected distribution (dashed) for RV constant objects is also shown for a comparison, and is normalized to the total number of objects that have $p > 10^{-3}$. The match between the expected distribution and the histogram is reasonable (cf. Section 3.1), indicating that our uncertainty estimates in RV values are also reasonable.

right-hand side, we find the χ^2 probability of the fit increases to 0.9. This, in turn, indicates that our uncertainties in RV values are reasonable, and an additional systematic error is not necessary in this analysis. This assertion is supported by the reanalysis of BD RVs, obtained by Joergens (2006b) using the same instrumental set-up as ours, by Maxted & Jeffries (2005).

The boundary ($p = 10^{-3}$) between the RV variable and the RV constants seems somewhat arbitrary, but here we simply adopt the definition of Maxted & Jeffries (2005). Based on this criterion, there are four objects which show significant RV variations (out of 17 samples) as one can see from the figure. They are USco 112, USco 128, USco 40 and USco 55, and considered as our preliminary binary/multiple candidates. We will discuss the binary fraction and the expected binary detection probability later in Section 4.

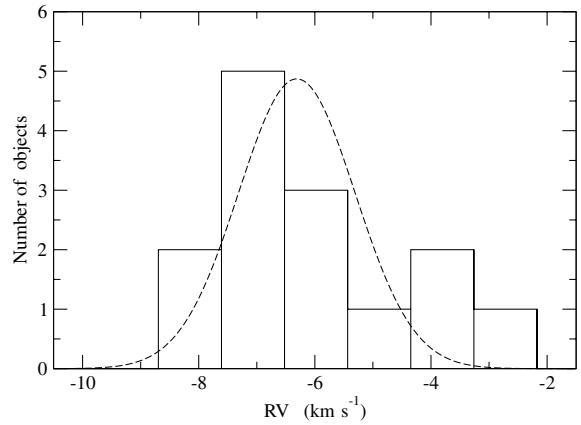

Figure 3. Histogram of the average heliocentric RVs of 14 UScoOB BD and VLM objects listed in Table 2 (excluding USco 121, a non-member). The Gaussian fit (dashed) of the RV distribution gives a s.d. of 1.0 km s^{-1} and the peak position of -6.3 km s^{-1}.

Finally, the histogram of $\overline{\mathrm{RV}}$ for the objects in UScoOB is given in Fig. 3. The total number of the objects is 14. Note that USco 121 is excluded from the graph since it is identified as a non-member of the UScoOB association based on the RV value (see Table 2). Muzerolle et al. (2003) also found it to be a likely non-member based on the RV and the low lithium abundance. The distribution of the RVs in the figure was fitted by a Gaussian function. We found that the s.d. and the peak position of the RV distribution are 1.0 and -6.3 km s^{-1}, respectively. The former is very similar to the s.d. (0.9 km s^{-1}) of the RV distribution of nine BDs and VLM objects in Chamaeleon I (Cha I) found by Joergens (2006a). They also studied the RV distribution of more massive 25 T Tauri stars in Cha I, and found the s.d. values (1.3 km s^{-1}) is not significantly different from that of the BDs and the VLM objects. Unfortunately, we do not have the RV measurements of the higher mass counter parts (T Tauri stars) in UScoOB. This is planned for future investigation since this is important for the study of the mass dependency of the kinematics in a young stellar cluster.

According to the hydrodynamical simulations of a low-mass star-forming cluster of Bate, Bonnell & Bromm (2003) which yields a stellar density of $\sim 10^3$ stars pc^{-3}, the rms dispersion (1D) of the stars and the BDs is 1.2 km s^{-1}. Similarly for the model with a higher stellar density ($\sim 10^4$ stars pc^{-3}), the rms dispersion is 2.5 km s^{-1} (Bate & Bonnell 2005). The s.d. of $\overline{\mathrm{RV}}$(1.0 km s^{-1}) found in our analysis is more comparable the lower stellar density model.

3.2 Rotational velocities

The rotational velocities of the objects were determined by measuring the widths of the cross-correlation functions of the target spectra against a template spectrum from an object which is known to have a very small rotational velocity. The line broadening of the targets is assumed to be dominated by rotational broadening. As in the cases for the RV measurements, LHS 49 is chosen as the template. Using its rotational period ($P \approx 83$ d Benedict et al. 1998) and radius ($R_* \approx 0.145$ R$_\odot$ from the VLTI measurement by Ségransan et al.

Downloaded from https://academic.oup.com/mnras/article-abstract/372/4/1879/1192749 by University of Sheffield user on 08 April 2019

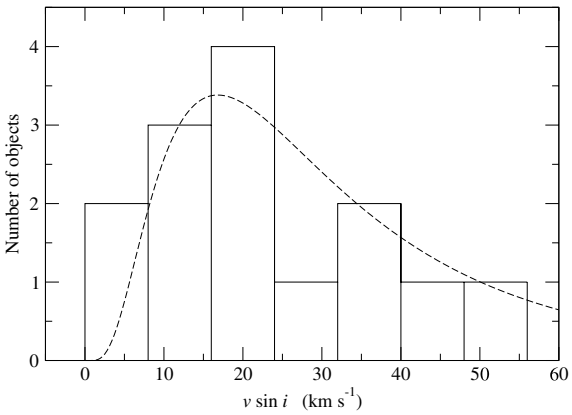

Figure 4. Histogram of the rotational velocities ($v \sin i$) of 14 UScoOB BD and VLM objects listed in Table 2 (excluding USco 121, a non-member). The lognormal fit (dashed) of the rotational velocity distribution gives a s.d. 27.8 km s^{-1} and the peak position 16.9 km s^{-1}.

2003), the rotational velocity of LHS 49 is estimated as $v \sin i = 2\pi R_*/P \approx 0.1$ km s^{-1}; negligibly small.

The width of the cross-correlation curves ($\sigma_{\rm CCF}$) are calibrated with the rotational velocities ($v \sin i$) by cross-correlating the template spectra against the same template spectra with added rotation (convolved with a given $v \sin i$), as done by, for example, Tinney & Reid (1998), Mohanty & Basri (2003) and White & Basri (2003). A linear limb-darkening law with a solar-like parameter ($\epsilon = 0.6$) was assumed in the formulation of the rotational profile described by Gray (1992, his equation 17.12). For each object, two measurements of rotational velocities are computed from two independent spectra obtained at different epochs. As for the RV measurements, the mean and the s.d. of the mean are used as the final rotational velocity and its uncertainty. The final results are recorded in Table 2. In general, our measurements are in good agreement with the earlier measurements of Muzerolle et al. (2003) and Mohanty, Jayawardhana & Basri (2005), given in Table 1. For example, Muzerolle et al. (2003) found $v \sin i = 16.8 \pm 2.7$ km s^{-1} for GY 5 while we found $v \sin i = 16.5 \pm 0.6$ km s^{-1}.

The range of $v \sin i$ found among our objects is 3.6–55.6 km s^{-1}, and a similar range is also found by Mohanty et al. (2005). Fig. 4 shows the histogram of $v \sin i$ distribution for the UScoOB objects (14 objects excluding USco 121, non-member). The lognormal fit of this distribution gives the peak position at 16.9 km s^{-1} with a s.d. $\sigma = 27.8$ km s^{-1}. Using the $v \sin i$ data in Joergens & Guenther (2001), the same histogram bin size used for UScoOB objects and a lognormal fit, we find the $v \sin i$ distribution of the BD and VLM stars (eight objects) in Cha I peaks at 15.4 km s^{-1}, and has the s.d. of 8.0 km s^{-1}. The peak of the distribution is similar to that of USco objects, but the s.d. of the distribution is much smaller than that of our USco objects. The difference may be due to the very small sample. A similar fit was applied to the $v \sin i$ distribution of 14 higher mass T Tauri stars in Cha I using the data of Joergens & Guenther (2001), and we found a peak at 17.0 km s^{-1} with a s.d. 25.9 km s^{-1} which are very similar to those of the USco BD candidates and VLM stars.

4 BINARY FRACTION

In Section 3.1, we found four out of 17 (excluding USco 121; non-member) objects show a statistically significant RV variation, indicating that they are binary/multiple candidates. In order to estimate the uncertainty in the binary/multiple fraction from this relatively small sample, we will follow the method used by Basri & Reiners (2006) who considered the binomial distribution, $P_{\rm B}(x, n, p)$ of x positive event out of n trials with the probability p for a positive event in each trial. In our case, $n = 17$ (the number of sample) and $x = 4$. The peak of $P_{\rm B}(4, 17, p)$ curve suggests the binary fraction of 24 per cent, as it should be ($4/17 = 0.24$). The uncertainties was estimated by plotting $P_{\rm B}(4, 17, p)$, and finding the values of p at which $P_{\rm B}$ reduced to e^{-1} of the peak value. In this analysis, we find the binary/multiple fraction along with the uncertainties of our sample to be $f = 24^{+16}_{-13}$ per cent.

Next, we investigate the range of semimajor axes of binaries (equivalently the range of binary periods) to which our RV survey is sensitive. For this purpose, we will consider the detection probability for binaries or the RV variables, given the time separations of two-epoch observations and the ranges of estimated primary masses (cf. Tables 1 and 2). The probability is calculated based on the simulated RV observations of binaries whose orbits are randomly selected from a model. A similar method was used by Maxted & Jeffries (2005) and Basri & Reiners (2006). The most important factors in determining the detection probability are the size of uncertainties in RV measurements (here we use the average $\sigma_{\rm RRV}$ from our observation), and the time separations of observations. The smaller the error in RV measurements, the larger the probability for a given binary orbit and a time separation of orbit. The larger the time separation of observations, the larger the upper limit of the semimajor axis to which an observation is sensitive. The average time separation of the two-epoch RV observations of our targets is 21.6 d. In the following, we will briefly discuss our model assumptions and parameters which are essentially the same as those of Maxted & Jeffries (2005) but with some simplifications.

There are six basic parameters in our Monte Carlo simulation: primary mass (M_1), mass ratio (q), eccentricity (e), orbital phase (ϕ), orbital inclination (i) and longitude of periastron (λ). The primary mass M_1 is assigned from the adopted mass of the targets in Table 1, with a uniform random deviation of $\pm$ 0.002 M$_\odot$. The mass ratio is assumed to be uniformly distributed between $q = 1$ and 0.2. The eccentricity e is assumed to be zero (circular orbits). Both Maxted & Jeffries (2005) and Basri & Reiners (2006) found that the detection probability is insensitive to the assumed distribution of q and e. Although $e = 0$ is assumed here, a non-zero e distribution would result in a slightly higher detection probability for wider separation systems (cf. Maxted & Jeffries 2005). The orbital phase is randomly chosen between 0 and 1. The inclination i is randomly chosen from the cumulative distribution of cos i. The longitude of periastron λ is not necessary since we assumed $e = 0$.

In order to compute the detection probability as a function of semimajor axis a, we take the following procedure: (1) for each object in our targets, we randomly select 10^5 binaries using the assumption stated above for a given value of a, and compute the RV of the primary (V_1), (2) evolve the orbit by the time separation of the RV measurements used in the observations for this object, and take another simulated measurement of RV (V_2), (3) from V_1, V_2 and the average uncertainty in RV ($\sigma_{\rm RRV}$) from the observations, we compute the χ^2 probability p, and flag the trial as a detection if $p < 10^{-3}$ as done for the real data, (4) find the fraction of detections out of all random trials, (5) repeat steps 1–4 for the range of a between 10^{-3} and 10 au and (6) repeat step 5 for the all targets, and find the detection probability averaged over all targets as a function of a.

The result of the simulation is shown in Fig. 5. The detection probability curve shown here is very similar that of Basri & Reiners (2006) for a constant time separation (20 d) case (see their fig. 4). The

Downloaded from https://academic.oup.com/mnras/article-abstract/372/4/1879/1192749 by University of Sheffield user on 08 April 2019

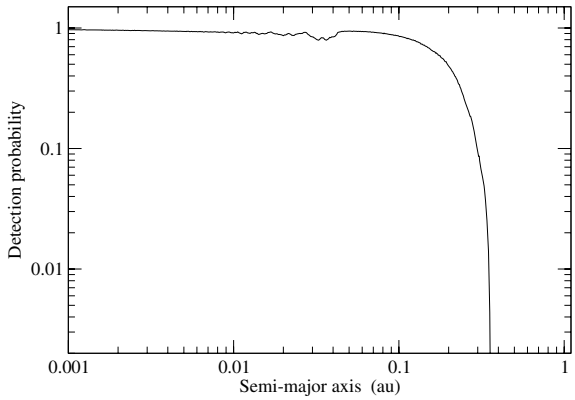

Figure 5. The binary detection probability (solid) as a function of the semi-major axis (a), based on Monte Carlo simulations of RV measurements, is shown. For each object in our target list, the simulation was performed using the time separation (Δt) actually used in our two-epoch observations (cf. Table 2) and the estimated primary mass (cf. Table 1). The final detection probability is obtained by averaging over the simulated observations of all the objects. The average time separation in the two-epoch observations is ~21.6 d, and the average uncertainty in RV is 0.42 km s^{-1}. The probability remains fairly constant up to $a \approx 0.1$ au, and it rapidly decreases beyond $a \approx 0.3$ au. The 80 per cent detection probability is achieved for binaries with $a < 0.1$ au.

probability remains fairly constant up to $a \approx 0.1$ au, and it rapidly decreases beyond $a \approx 0.3$ au. This turning point will increase if we had used larger time separations in our observation. From this figure, we find that the 80 per cent detection probability up to for binaries with $a < 0.1$ au, given our time separations and the average uncertainty (~0.42 km s^{-1}) in the RV measurements.

Alternatively, the RV variations seen in the binary candidates above may be caused by a type of stellar pulsations predicted by Palla & Baraffe (2005). They studied the non-adiabatic, linear instability of VLM stars and BD during the deuterium burning phase in the core, and found unstable fundamental modes in the time-scale between ~1 and ~5 h for the object mass from 0.02 and 0.1 M$_\odot$. By using their pulsation periods and by assuming that the pulsation amplitude is 5 per cent of the radius of the objects, we find that the expected RV variation can be >6 km s^{-1}. As mentioned in Section 2, for each object at a given night, two separate spectra are obtained consecutively (with time separations of ~0.5 h). We have measured the RV from each spectrum to check if there is a large jump in the RV measurements on a short time-scale. The size of the shifts in the RV values measured in the two consecutive spectra are found in between 0.02 ± 0.10 (USco 128) and 2.04 ± 1.67 km s^{-1} (USco 66), and the average size of the shifts 0.36 km s^{-1}, which is much smaller than the expected RV variation based on the models of Palla & Baraffe (2005); hence, we found little indication of the pulsations in our sample.

5 CONCLUSIONS

We have presented two-epoch RV survey of 18 young BDs and VLM stars (0.02 M$_\odot$ < M_* < 0.1 M$_\odot$) in UScoOB and ρ Oph dark cloud core using the high-resolution UVES echelle spectroscopy at VLT. The average time separation of RV measurements is 21.6 d, and our RV survey is sensitive to binaries with separation smaller than 0.1 au. One of our targets, USco 121, is most likely a non-member of the UScoOB association based on the deviation of the RV from the result of the population in the association. A similar conclusion was found by Muzerolle et al. (2003) from their RV study and the low lithium abundance.

We found four (USco 112, USco 128, USco 40 and USco 55) out of 17 objects as our binary/multiple candidates. This corresponds to the binary fraction of 24^{+16}_{-13} per cent for the binary separation $a <$ 0.1 au. The recent high-resolution imaging survey of BDs and VLM objects (M5.5–M7.5) in the UScoOB by Kraus et al. (2005), which was not known to authors at the time of our observation: 2004 April–May, confirms that USco 55 and USco 66 are multiple systems, and USco 109 is most likely a multiple system. Their projected separations are $a > 4.0$ au which is well above our sensitivity limit of 0.1 au; therefore, it is not surprising that we did not identify USco 66 and USco 109 as multiples. Interestingly, we also found USco 55 as a candidate for a multiple system. This may indicate that it is a triple system with one of the objects located within 0.1 au of the primary. In addition, we identify USco 112 and USco 128 as binary candidates, but they did not find them as multiples. Further they found USco 67, USco 75, USco 130 and USco 132 as non-multiple, as did we.

We found the RV dispersion (1.0 km s^{-1}) of the objects in UScoOB is very similar to that of the BDs and VLM stars in Cha I previous study by Joergens (2006a). The rotational velocities ($v \sin i$) of the samples were also measured. The distribution of $v \sin i$ for the UScoOB objects peaks around 16.9 km s^{-1} which is also similar to that of the Cha I population found by Joergens (2006a); however, the dispersion of $v \sin i$ for the UScoOB objects (27.8 km s^{-1}) is found to be much larger than that of the Cha I objects (8.0 km s^{-1}).

Follow-up spectroscopic observations of the binary candidates presented here are planned in near future. There are only a few RV variable binary candidates identified in earlier surveys (Guenther & Wuchterl 2003; Kenyon et al. 2005; Joergens 2006b). As Burgasser et al. (2006) point out most of the current RV and imaging surveys use samples from magnitude-limited survey, but one should attempt to use the samples from volume-limited survey in order to find a correct statistics on binary parameters more straightforwardly, that is, without correcting for bias. It is possible that our binary fraction is an overestimate since we are biased to brighter objects. However, the lack of a double-line system suggests that a primary-to-secondary luminosity ratio of ≫1 for the RV variables found in this paper.

ACKNOWLEDGMENTS

We would like to thank the anonymous referee for constructive comments and suggestions for improving the clarity of the manuscript. We also thank the staff of VLT of the ESO for carrying out the observations in service mode. RK is grateful for Rob Jeffries and Tim Naylor for helpful suggestions on the data analysis presented in this paper. We also thank Matthew Bate for providing us valuable comments on the manuscript. This work was supported by PPARC rolling grant PP/C501609/1.

REFERENCES

Ardila D., Martín E., Basri G., 2000, AJ, 120, 479
Bailer-Jones C. A. L., 2004, A&A, 419, 703
Baranne A. et al., 1996, A&AS, 119, 373
Basri G., Martín E. L., 1999, AJ, 118, 2460
Basri G., Reiners A., 2006, AJ, 132, 663
Bate M. R., Bonnell I. A., 2005, MNRAS, 356, 1201
Bate M. R., Bonnell I. A., Bromm V., 2002a, MNRAS, 332, L65

Downloaded from https://academic.oup.com/mnras/article-abstract/372/4/1879/1192749 by University of Sheffield user on 08 April 2019

Bate M. R., Bonnell I. A., Bromm V., 2002b, MNRAS, 336, 705
Bate M. R., Bonnell I. A., Bromm V., 2003, MNRAS, 339, 577
Benedict G. F. et al., 1998, AJ, 116, 429
Bouy H., Moraux E., Bouvier J., Brandner W., Martín E. L., Allard F., Baraffe I., Fernández M., 2006, ApJ, 637, 1056
Burgasser A. J., McElwain M. W., Kirkpatrick J. D., 2003, AJ, 126, 2487
Burgasser A. J., Reid I. N., Siegler N., Close L., Allen P., Lowrance P., Gizis J., 2006, in Reipurth B., Jewitt D., Keil K., eds, Protostars and Planets V. Univ. Arizona Press, Tucson, in press (astro-ph/0602122)
Close L. M., Siegler N., Freed M., Biller B., 2003, ApJ, 587, 407
de Zeeuw P. T., Brown A. G. A., de Bruijne J. H. J., Hoogerwerf R., Lub J., Le Poole R. S., Blaauw A., 1997, in Battrick B., ed., ESA SP-402, Hipparcos Venice '97. ESA Publications Division, Noordwijk, p. 495
de Zeeuw P. T., Hoogerwerf R., de Bruijne J. H. J., Brown A. G. A., Blaauw A., 1999, AJ, 117, 354
Duquennoy A., Mayor M., 1991, A&A, 248, 485
García-Sánchez J., Weissman P. R., Preston R. A., Jones D. L., Lestrade J.-F., Latham D. W., Stefanik R. P., Paredes J. M., 2001, A&A, 379, 634
Gizis J. E., Reid I. N., Knapp G. R., Liebert J., Kirkpatrick J. D., Koerner D. W., Burgasser A. J., 2003, AJ, 125, 3302
Gray D. F., 1992, The Observation and Analysis of Stellar Photospheres. Cambridge Univ. Press, Cambridge
Guenther E. W., Wuchterl G., 2003, A&A, 401, 677
Horne K., 1986, PASP, 98, 609
Joergens V., 2006a, A&A, 448, 655
Joergens V., 2006b, A&A, 446, 1165
Joergens V., Guenther E., 2001, A&A, 379, L9
Kenyon M. J., Jeffries R. D., Naylor T., Oliveira J. M., Maxted P. F. L., 2005, MNRAS, 356, 89
Kraus A. L., White R. J., Hillenbrand L. A., 2005, ApJ, 633, 452
Luhman K. L., 2004, ApJ, 614, 398
Luhman K. L., Rieke G. H., 1999, ApJ, 525, 440
Martín E. L., Barrado y Navascués D., Baraffe I., Bouy H., Dahm S., 2003, ApJ, 594, 525
Maxted P. F. L., Jeffries R. D., 2005, MNRAS, 362, L45
McCaughrean M. J., Andersen M., 2002, A&A, 389, 513
Mohanty S., Basri G., 2003, in Brown A., Harper G. M., Ayres T. R., eds, The Future of Cool-Star Astrophysics: 12th Cambridge Workshop on Cool Stars, Stellar Systems, and the Sun, Univ. Colorado, Boulder, p. 683
Mohanty S., Jayawardhana R., Basri G., 2005, ApJ, 626, 498
Muzerolle J., Hillenbrand L., Calvet N., Briceño C., Hartmann L., 2003, ApJ, 592, 266
Padoan P., Nordlund Å., 2002, ApJ, 576, 870
Palla F., Baraffe I., 2005, A&A, 432, L57
Pinfield D. J., Dobbie P. D., Jameson R. F., Steele I. A., Jones H. R. A., Katsiyannis A. C., 2003, MNRAS, 342, 1241
Reipurth B., Clarke C., 2001, AJ, 122, 432
Ségransan D., Kervella P., Forveille T., Queloz D., 2003, A&A, 397, L5
Siegler N., Close L. M., Cruz K. L., Martín E. L., Reid I. N., 2005, ApJ, 621, 1023
Stassun K. G., Mathieu R. D., Valenti J. A., 2006, Nat, 440, 311
Tinney C. G., Reid I. N., 1998, MNRAS, 301, 1031
Udry S., Mayor M., Queloz D., 1999, in Hearnshaw J. B., Scarfe C. D., eds, ASP Conf. Ser. Vol. 185, IAU Colloq. 170: Precise Stellar Radial Velocities. Astron. Soc. Pac., San Francisco, p. 367
White R. J., Basri G., 2003, ApJ, 582, 1109
Whitworth A. P., Zinnecker H., 2004, A&A, 427, 299
Wilking B. A., Greene T. P., Meyer M. R., 1999, AJ, 117, 469

This paper has been typeset from a TEX/LATEX file prepared by the author.

Downloaded from https://academic.oup.com/mnras/article-abstract/372/4/1879/1192749 by University of Sheffield user on 08 April 2019